Multilayer Transparent Top Electrode for Solution Processed Perovskite/Cu(In,Ga)(Se,S)$_2$ Four Terminal Tandem Solar Cells

Yang (Michael) Yang,[†,§] Qi Chen,[†,‡,§] Yao-Tsung Hsieh,[†,‡] Tze-Bin Song,[†,‡] Nicholas De Marco,[†,‡] Huanping Zhou,[*,†,‡] and Yang Yang[*,†,‡]

[†]Department of Materials Science and Engineering, University of California, Los Angeles, California 90095, United States and [‡]California NanoSystems Institute, University of California, Los Angeles, California 90095, United States. [§]These authors contributed equally to this work.

ABSTRACT Halide perovskites (PVSK) have attracted much attention in recent years due to their high potential as a next generation solar cell material. To further improve perovskites progress toward a state-of-the-art technology, it is desirable to create a tandem structure in which perovskite may be stacked with a current prevailing solar cell such as silicon (Si) or Cu(In,Ga)(Se,S)$_2$ (CIGS). The transparent top electrode is one of the key components as well as challenges to realize such tandem structure. Herein, we develop a multilayer transparent top electrode for perovskite photovoltaic devices delivering an 11.5% efficiency in top illumination mode. The transparent electrode is based on a dielectric/metal/dielectric structure, featuring an ultrathin gold seeded silver layer. A four terminal tandem solar cell employing solution processed CIGS and perovskite cells is also demonstrated with over 15% efficiency.

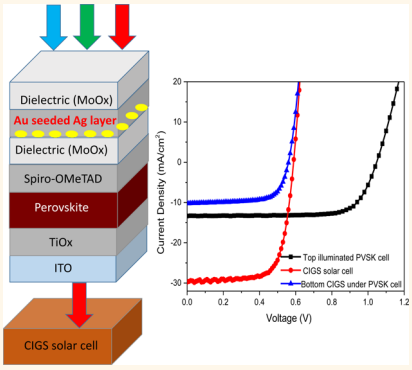

KEYWORDS: perovskite · transparent electrode · tandem · dielectric/metal/dielectric · solar cell

Sunlight is one of the most abundant renewable energy sources on our planet, yet it remains poorly utilized. Over the past decades, people have sought alternative materials for photovoltaic devices that feature both low cost and high efficiency, *e.g.*, organic photovoltaics (OPV),[1−6] Dye Sensitized Solar Cells (DSSC),[7−10] *etc.* The recent advent of the organic−inorganic hybrid halide perovskite (PVSK) has led to rapid progress of photovoltaic/optoelectronic devices.[11−25] In addition, the capability for the simple film deposition through either vacuum or solution-based methods makes it a tremendous candidate for the future solar cell market.

As the efficiency of the PVSK solar cell is approaching its theoretical limitation, it is necessary to start to consider how to go beyond the S-Q limit. There are two major losses that currently prevent a higher PCE from being obtained in single junction PVSK devices in (1) the below band gap transmission and (2) the thermal relaxation of hot charge carriers. The band gap of semiconductors can be reduced to enhance absorption and increase the short circuit current (J_{sc}), while the ultrafast hot carrier relaxation process sets the limit of the open circuit voltage (V_{oc}) to be the band gap. The most promising method to circumvent both effects is to construct a tandem junction device consisting of a bottom cell fabricated based on prevailing solar cell techniques *e.g.*, Si and CIGS, and a top cell with a higher bandgap absorber. Up to date, this method has had limited success due to the absence of suitable materials to produce high efficiency top cells compatible with current photovoltaic (PV) technology as bottom cells. The rapid progress of the organic−inorganic hybrid perovskite materials with ~1.55 eV band gap is a potential candidate to be utilized as the top cell to further improve the state-of-the-art of the solar cell technology. This family of materials is gifted the most attractive optoelectronic characteristics as an ideal standalone

* Address correspondence to yangy@ucla.edu, happyzhou@ucla.edu.

Received for review May 27, 2015 and accepted June 21, 2015.

Published online June 22, 2015
10.1021/acsnano.5b03189

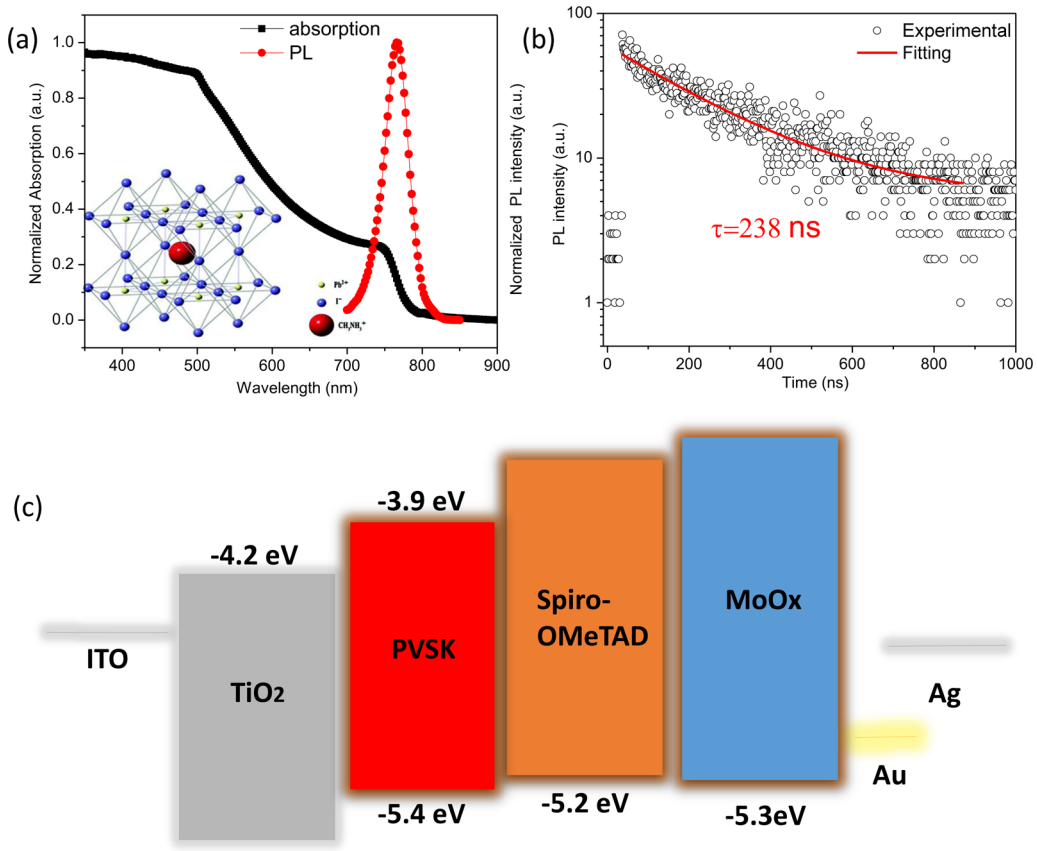

Figure 1. Basic optical and electrical characteristic of halide perovskite material and its photovoltaic device. The absorption and photoluminescence (PL) spectra (a); time-resolved PL measurement (b); and energy band positons of n-i-p photovoltaic device (c).

absorber, including a high absorption coefficient, tunable bandgap, long carrier diffusion length and more.[20,26] Notably, hybrid perovskites also show a sharp absorption edge with small Urbach energy.[27] Figure 1a shows the chemical structure of PVSK, as well as the linear optical absorption and photoluminescence spectra of the PVSK material. The absorption edge is approximately 800 nm with a corresponding optical band gap of 1.55 eV. It exhibits strong absorption above the band gap as well as a sharp optical transition at the band edge. Most of recent theoretical calculations indicate a direct band gap structure for the perovskite semiconductor.[28] Figure 1b shows the results of transient PL measurement of the typical PVSK film in our study, which exhibits mono exponential decay with carrier lifetime of 238 ns. It is relatively long for the typical direct band gap material, which might be related with its unique band structure or excite states physics that are not fully understood yet. However, it indicates at least the nonradiative decay channels are considerably suppressed. Such features not only explain the superior PVSK single junction device but also imply the PVSK material is a good candidate to be implemented into a tandem structure.

Conventional inorganic solar cells, *e.g.*, CIGS solar cell, are constructed from opaque substrates such as Mo, while PVSK solar cells are based on a transparent bottom electrode, *e.g.*, ITO or FTO, with p-i-n or n-i-p configuration. The energy band position for the generally adopted n-i-p PVSK solar cell is illustrated in Figure 1c; the values for the electron affinity and ionization potential refer to the previous study.[29] To make these two technologies compatible, the use of transparent top electrode for the PVSK cell is inevitable. In addition to the demands of a tandem device, a semitransparent PVSK solar cell itself is also attractive as it can potentially be applied to building-integrated photovoltaic (BIPV) applications.[30] To fulfill such demands, it is necessary to develop an effective and simple transparent top electrode compatible with PVSK solar cells.

Recent developments of transparent conductor technologies has enabled several systems to serve as a model for our design, *e.g.*, solution processed metal nanowires (Ag or Cu), conducting polymers and graphene, dielectric/metal/dielectric photonic structures, and more.[31−33] Most of these possibilities are obtainable through solution-processing or wet-transfer techniques.[31,34] Although proven to be successful in organic devices, these transparent conductors are challenging to implement into the PVSK system since the polar solvent used to disperse such transparent conductors usually dissolves the PVSK materials, as PVSK is a polar semiconductor. To this date, transparent top electrodes have been successfully applied in PVSK solar cells *via*

a limited number of approaches. A thin gold layer (~10 nm) has been reported *via* thermal evaporation to achieve a device PCE of 7.5%.[35] In another report, a transparent conducting adhesive was utilized to laminate a Ni mesh embedded within PET onto the perovskite solar cell to yield a decent PCE over 15%.[36]

The development of a dielectric/metal/dielectric (DMD) (MoO_x/Ag/MoO_x) structure as the semitransparent top electrode offers a compelling approach for the pursuit of a semitransparent PVSK top cell. As mentioned previously, PVSK materials and adjacent transport materials are chemically and mechanically unstable for the direct implication of solution processed top electrodes, *e.g.*, Ag NWs, carbon nanotubes, or sputtered metal oxides. In addition, deposition of DMD structures is based on simple thermal evaporation processes, which appear to be a cost-effective approach in comparison to the combined techniques of thermal evaporation of a buffer layer followed by sputtering of a metal oxide. Apart from the ease of processing, this method provides for judicious control over film thickness of each material to ensure reproducibility of the resulting device performance.

RESULTS AND DISCUSSION

This PVSK device employs the widely used n-i-p planar structure with compact TiO_2 as the electron transport layer (ETL), and Spiro-OMeTAD as the hole transport layer (HTL). Processing of the TiO_2 film was achieved at 150 °C, which is a rather low temperature for compact ETL materials. The PVSK layer is deposited on the top of TiO_2 through a two-step solution-processing technique, the details of which are included in the Methods section; the film morphology is given in Supporting Information Figure S1. Spiro-OMeTAD with ~350 nm thickness was subsequently deposited, serving as the HTL. We used thermally evaporated MoO_x as the dielectric material in the DMD structure due to the hole conducting nature and suitable band position of MoO_x compatible with Spiro-OMeTAD to provide for efficient hole extraction and transport. The band position of each layer is illustrated in Figure 1c. MoO_x is a commonly used hole transporting material in organic photovoltaic devices and silicon solar cell.[37,38] In this study, we also confirms that the Spiro-OMeTAD/MoO_x layer work as an effective hole selective layer. The device parameters of this type of device are almost comparable with the typical Spiro-OMeTAD/Au device, as shown in Supporting Information Figure S2. In addition, we also find that the MoO_x metal oxide affects the surface properties of the original Spiro-OMeTAD hole transport materials, providing improved adhesion for the following metal deposition. The entire top electrode is then completed by subsequent deposition of a thin metal layer and an additional MoO_x dielectric layer for optical interference to enhance the transparency. The metal film has strong reflection even at 11 nm thickness; the top MoO_x layer can be considered as the antireflection layer. However, it is challenging to achieve antireflection for the whole spectra, and hence, the optimal thickness of this layer depends on particular photovoltaic system.

The most crucial part of the transparent electrode is the metal layer stacking in-between the dielectric materials, which determines the trade-off between the transparency and the conductivity of the entire top electrode. Most traditional DMD structures employ a silver, and occasionally gold, middle layer.[39−41] We initially used a thin Ag layer, due to its high visible transparence and low cost. The silver thin film deposited on the dielectric material is likely to form isolated clusters for the initial few nanometers of deposition. Therefore, the percolation thickness (thickness at which the film becomes continuous) of silver must exceed the threshold, where the following coalescence and film growth process can be completed to form a continuous network. Attempts to improve film quality during metal deposition consider not only film thickness, but other deposition parameters as well. For instance, on the basis of the fast evaporation rate (>5 nm/s) of silver, a more continuous film with higher conductivity at a similar range of film thickness can be achieved. This is likely due to the rather sufficient number of vapor atoms or molecules that condense and merge together to establish a continuous network on the substrate. However, in PVSK solar cells, such a fast deposition rate can easily damage the Spiro-OMeTAD and even the PVSK film. In addition, substrate temperature and roughness have also been found to play an important role in certain circumstances, which increases the complexity of this technology and reduces the device performance, yield and reproducibility. In our case, it is desirable to achieve Ag film percolation thicknesses as low as possible using a mild deposition method, so as to minimize optical losses from absorption by the electrode itself.

Interestingly, we found that in an ultrathin gold seed layer (~1 nm) beneath a silver film provides an ideal solution for improving the adhesion and reducing the percolation thickness of the metal film sandwiched between the dielectric structures. This results in a dramatic change of silver film morphology. As shown in Figure (2a−c), without gold seed layer, the silver film is not continuous at 11 nm, presenting isolated metal inlands, and the film is highly resistive. With the same metal film thickness, it becomes continuous across the entire film by inserting only 1 nm gold seed layer as shown in Figure 2b. In contrast, the pure gold thin film with same thickness also shows noncontinuous feature, the film consists of tiny isolated gold islands as shown in Figure 2c. This result suggests that a substantially different nucleation and growth mode of the metal film occurs during the evaporation process by incorporating alternative gold seeding layer.

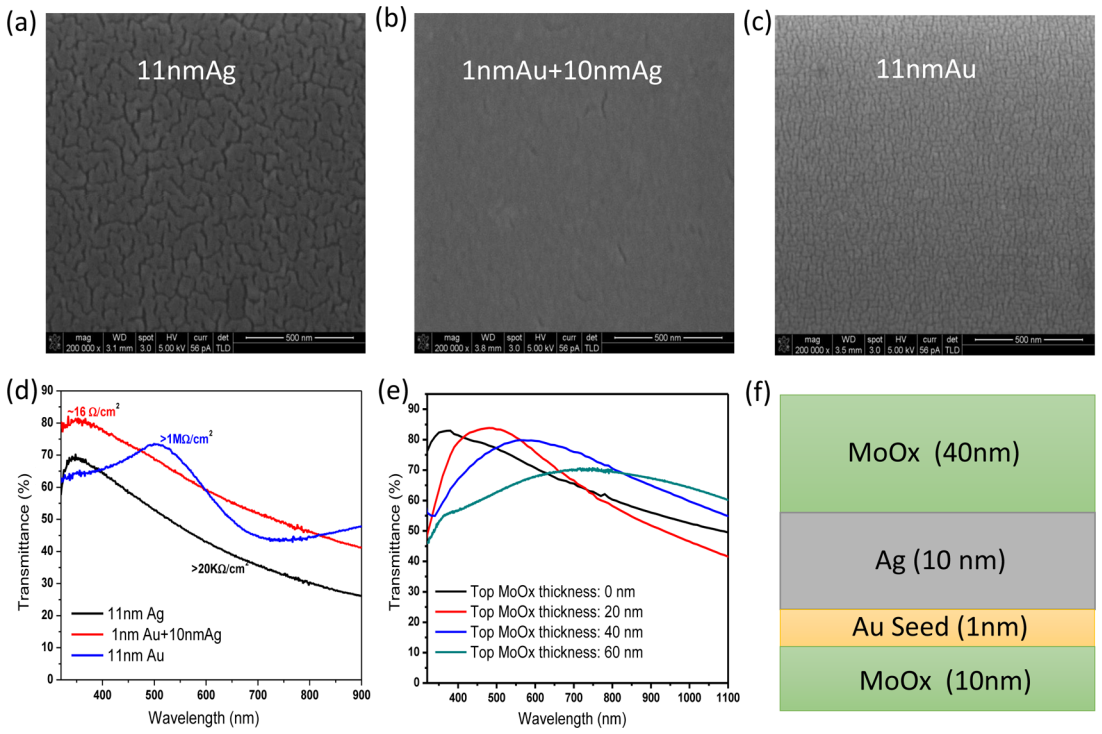

Figure 2. Characterization of multilayer transparent top electrode. The film morphology of pristine silver (a), gold seeded silver (b) and pristine gold (c) layer with same metal thickness; the transparence and conductivity of pristine silver, gold seeded silver, and pristine gold film (d); the transparency of the multilayer electrode with different MoO_x topping layer thickness (e); the optimized parameters for the multilayer transparent electrode used in PVSK solar cell (f).

Generally, in case of metal films nucleation, the adatoms tend to bound to each other instead of bounding to the substrates, and therefore, they grow *via* Volmer–Weber (island) mode. It explains the noncontinuous film appearing in both cases of the individual Au and Ag deposition below the critical thickness. While an improved wetting of the substrate has proven to be favorable for the Frank–van der Merwe (layer-by-layer) growth, it is the reason for the widely used "trick" that Cr seed is predeposited before the subsequent Au deposition in many electric devices. In our study, the gold is predeposited on the substrate and form islands, the subsequent adsorbed Ag atoms/molecules (adatoms) may have the chance to be more strongly bound to the substrate than to the nearby gold islands. The interaction between Ag and substrate is energetically more favorable than the Ag–Au interaction, since gold has higher surface energy. The growth mode transitions from Volmer–Weber (island) mode in homogeneous Ag or Au thin film to the Frank–van der Merwe (layer-by-layer) mode in the Au/Ag heterostructure thin film. Facilitated by the gold seed, the silver film with only 10 nm result in a continuous film, and such a small percolation thickness will ensure good optical transparency as well as the conductivity of the thin film electrode.

As shown in Figure 2d, the conductivity of the corresponding silver film improves several orders of magnitude from 20KΩ/□ (11 nm Ag) to around 16 Ω/□ (1 nm Au + 10 nm Ag). This is presumably because the isolated metal islands are well connected to form charge conduction pathways. The gold seeded silver film is also superior when compared to the pure gold film in terms of conductivity and transparency, where the same thickness of gold is very resistive and exhibits low transmittance in the visible region due to the strong plasmonic scattering effect of the gold nano domains.[42] A dielectric toping layer was used to further improve the transmittance of the electrode. All the dielectric materials in principle can serve this function so long as they possess a large band gap to avoid optical absorption (*e.g.*, LiF).[35] Here, we employ MoO_x as the top layer due to its ease of processing, without changing the thermal evaporation source. The transmittance spectrum can be tuned by different MoO_x thicknesses to match the absorption spectra of the active layer, as shown in Figure 2e. The final optimized parameters of this D/M/D transparent top electrode is illustrated in Figure 2f. The transmittance is particularly high from 550 to 800 nm, within which the PVSK material actively absorbs photons.

The architecture of the top illuminated semitransparent PVSK solar cell as well as the cross-section image of each layer are shown in Figure 3a. The IV curve of the optimized championing device is shown in Figure 3b, delivering a very good device performance of 11.5% power conversion efficiency (PCE). As a reference, the "regular" PVSK solar cell with Spiro-OMeTAD as hole transporting layer and ~100 nm Au

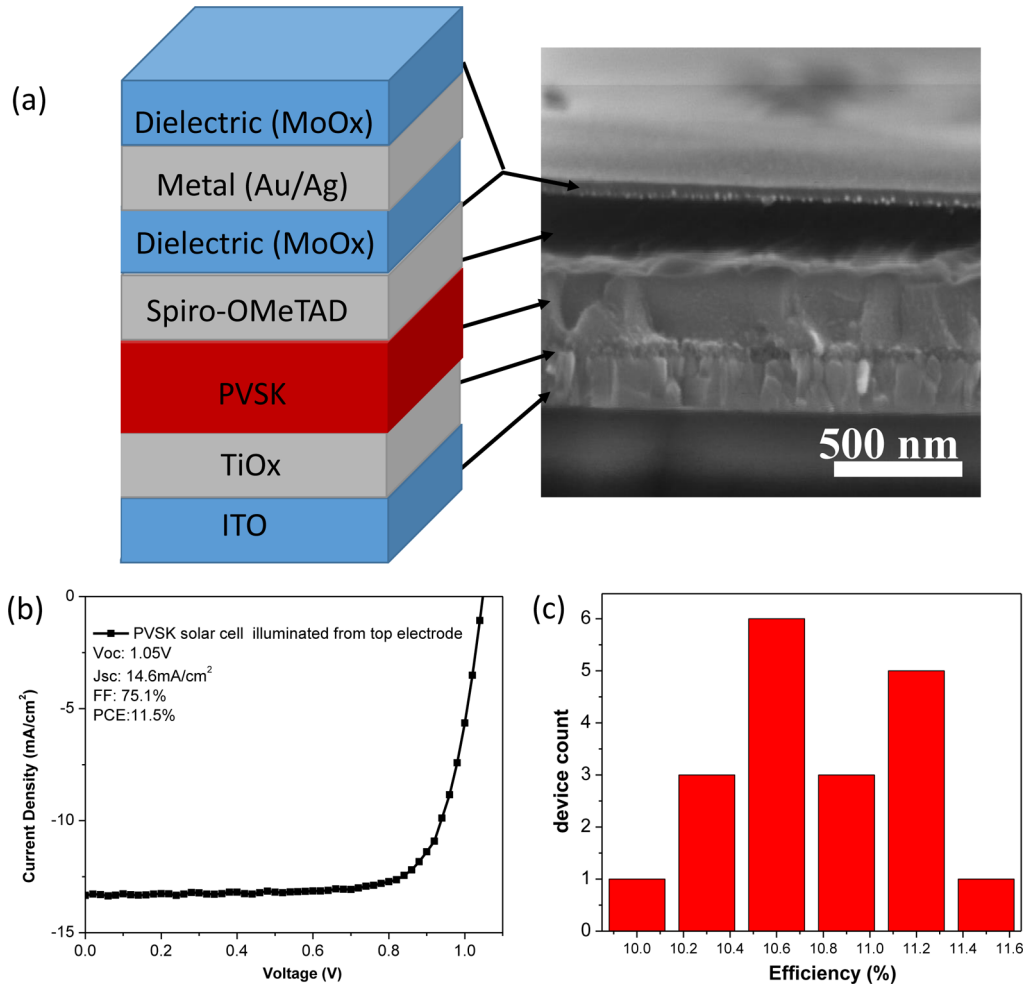

Figure 3. Device structure and performance of top illuminated PVSK solar cell. The schematic and TEM cross-sectional image of the photovoltaic device (a); *J*−*V* curve of the optimized device (b); the statistic of the device efficiency (c).

electrode is also fabricated and shows average power conversion efficiency of ~16.5%; the IV curve of the typical PVSK solar cell with regular electrode is included in Supporting Information Figure S2. The fill factor (FF) of the top illuminated PVSK cell achieves 75%, which is comparable to the best performing PVSK solar cells made with regular metal electrodes. The device performance distribution is given in Figure 3c. The open circuit voltage (V_{oc}) reached as high as 1.05 V. This is also a reasonably high value considering that the photoinduced excess carrier concentration inside the semitransparent PVSK is slightly lower than that of PVSK in regular devices, so that the quasi Fermi level splitting is slightly reduced. The high FF and V_{oc} both indicate that the sheet resistance of this D/M/D transparent electrode is low enough to avoid the resistive losses. The short circuit current (J_{sc}) is lower than that in the regular device due to the transmittance loss from the top electrode, achieving a value of 14.6 mA/cm^2, which is approximately 70% of that seen in typical PVSK photovoltaic devices. Such photocurrent loss correlates with the overall transmittance of the D/M/D transparent electrode.

On the basis of this D/M/D transparent top electrode, a four-terminal tandem solar cell employing a solution processed CIGS bottom cell was also demonstrated. The CIGS bottom cell was obtained following previous procedures,[43] and yields a V_{oc} of 0.59 V, J_{sc} of 29.8 mA/cm^2, FF of 70.7% and overall PCE of 12.4%. It must be noted that the top and bottom cell should have an approximately equal PCE in order to maximize the benefit of using a tandem device instead of a single junction. Hence, solution processed CIGS bottom cells and PVSK top cells are believed to be a good combination for a tandem structure. The four terminal device configuration is shown in Supporting Information Figure S3, the device is illuminated from the D/M/D electrode, and the IV curve of top and bottom cell were measured separately. The CIGS bottom cell underneath the top cell shows an efficiency of 4.0%, with J_{sc} of 10.2 mA/cm^2, V_{oc} of 0.56 V and FF of 69.6%. The current−voltage curves and the external quantum efficiency (EQE) curves of the top PVSK cell, unfiltered CIGS solar cell, and CIGS bottom cell underneath the PVSK cell are shown in Figure 4a,b. All corresponding device parameters are included in Table 1. The four-terminal tandem

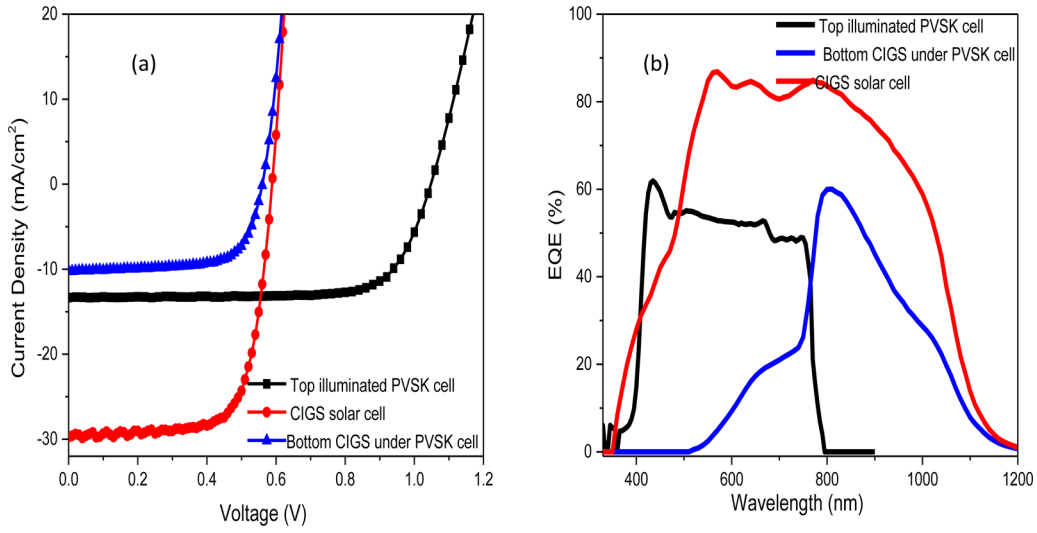

Figure 4. Device characterization of solution processed PVSK, CIGS, and the four terminal tandem photovoltaic devices. The *J*−*V* curve characterization of top illuminated PVSK, CIGS, and CIGS cell under the PVSK device (a); the EQE measurement of top illuminated PVSK, CIGS, and CIGS cell under the PVSK device (b).

TABLE 1. Outcomes of Device Performance of Top Illuminated PVSK, CIGS, and the Bottom CIGS Cell under the PVSK Device

	V_{oc} (V)	J_{sc} (mA/cm^2)	FF (%)	PCE (%)
PVSK Top cell Illuminated from D/M/D top electrode	1.05	14.6	75.1	11.5
CIGS solar cell	0.59	29.8	70.7	12.4
CIGS under PVSK cell	0.56	10.2	69.6	4.0
Four-terminal tandem				15.5

device efficiency is realized by adding the device efficiency of the top PVSK cell and the bottom CIGS cell when underneath the PVSK device. With an 11.5% efficient top illuminated PVSK cell, the efficiency of the solution processed CIGS solar cell was further enhanced to 15.5%, which was a 34.8% improvement compared with the PVSK cell. The ease of processing for both the PVSK and CIGS active layers also ensures a low cost of production for this technology. It is noted that a mechanically connected tandem solar cell employing coevaporated CIGS and solution processed PVSK has also been demonstrated with decent power conversion efficiency.[44] It is worth mentioning that both the PVSK and CIGS cell was used without an antireflection coating. Thus, the performance of tandem device should be further improved through incorporation of such photonic structures. The optical design parameters of such an antireflection coating will be different from that for a single junction device. Only the photons with energy below the perovskite band gap and bigger than CIGS band gap need to be considered for the bottom CIGS cell, which could lead to a more effective antireflection coating than that used in the regular CIGS solar cell.

CONCLUSION

In summary, we have successfully demonstrated a multilayer transparent top electrode for hybrid halide perovskite solar cells. The electrode employs the conventional dielectric/metal/dielectric structure featuring an ultrathin gold seeding layer underneath the silver layer. The gold seeded silver film shows significantly improved conductivity and optical transparency compared with pristine Ag or Au due to modification of the wetting properties of the metal deposition. The semitransparent perovskite solar cell illuminated from this multiplayer top electrode performs well with 11.5% efficiency and exhibits almost no loss of V_{oc} and FF compared with the regular device. This perovskite top cell was further connected with a solution processed CIGS bottom cell and measured as a four terminal tandem device, delivering a combined power conversion efficiency 15.5%. Our work not only demonstrates a simple processing method for a transparent top electrode of perovskite solar cells, but also shows a promising route to further improve current solar cell efficiency through the use of tandem perovskite/CIGS solar cell structures.

METHODS

PVSK Film Formation and Device Fabrication. Methylammonium iodide (CH_3NH_3I, MAI), methylammonium chloride (CH_3NH_3Cl, MACl), and the TiO_2 nanocrystals were synthesized following the approaches described elsewhere.[15] All the chemicals were used as received without any further purification including PbI_2 (99.999%, Sigma-Aldrich), HI (57 wt % in water, Aldrich), HCl, CH_3NH_2 (33 wt % in absolute ethanol, Sigma-Aldrich), $TiCl_4$, titanium diisopropoxide bis(acetylacetonate) 75% in isopropyl

alcohol (TiAcac, Sigma-Aldrich), spiro-OMeTAD (Lumtec), dimethylformamide (DMF), Li-bis(trifluoromethanesulfonyl) imide (Li-TFSI, Sigma), diethyl ether, acetone, isopropyl alcohol, acetonitrile, ethanol, 2-methoxyethanol, and benzyl alcohol. ITO or glass substrates (for PL measurements) were sequentially washed with isopropyl alcohol, acetone, distilled water and ethanol. The ETL was subsequently coated on ITO substrates with a TiAcac stabilized TiO_2 solution and annealed at 150 °C for 30 min in air. PbI_2 (dissolved in DMF, 400 mg/mL) was spin-coated on top of ITO/TiO_2 substrate at 2500 rpm for 30 s. Then dissolved in 2-propanol, a mixture of MAI/MACl (50 mg/mL, 5 mg/mL) was spin-coated on top of the dried PbI_2 layer at room temperature at 2000 rpm for 30 s in the dry air (at Dew Point of −70 °C). All of the films were annealed in the air at 135 °C for desired time. A hole transport layer (HTL) solution was coated on the perovskite film at 3000 rpm for 30 s, where a spiro-OMeTAD/chlorobenzene (90 mg/1 mL) solution was employed with addition of 45 μL of Li-TFSI/acetonitrile (170 mg/1 mL) and 10 μL of tBP. Finally, the counter electrode was deposited by thermal evaporation of gold under a pressure of $5 \times 10-5$ Torr. The active area was 0.108 cm^2. The as-fabricated reference device depicts from the bottom to the top, the 150 nm thick ITO electrode, 40 nm of TiO_2, 350 nm of perovskite, 200 nm of spiro-OMeTAD, and 100 nm of gold. The fabrication of solution processed CIGS solar cell follows previous work demonstrated in this study.[43] The transparent top electrode based device adopts all the device fabrication parameters as the reference device except replacing the Au electrode by multilayer top electrodes. The MoO_x/Au/Ag/MoO_x multilayer top electrode is deposited subsequently with thermal evaporation method, with the thickness of 10, 1, 10, and 40 nm, respectively. The evaporation rates for each layer are 0.1, 0.02, 0.1, and 0.1 nm/s, respectively.

Optical Characterization. The absorptions of different transparent electrodes and the PVSK film are measured with Hitachi UV−vis spectrometer in the transmission mode. The PL measurement is conducted with HORIBA fluorescence spectrometer, and the transient PL is measured using PicoQuant time correlated single photon counter.

Device Measurement. The current−voltage ($J-V$) measurements of the photovoltaic devices were conducted using a Keithley 236 Source-Measure unit. A xenon lamp with an AM1.5G filter (NEWPORT) simulated 1 sun conditions, and the light intensity at the sample was 100 mW/cm^2, calibrated with a Mono-Si photodiode with KG-5 color filter. The reference diode is traceable to NREL certification. EQE measurements were conducted with an integrated EQE system from EnliTech. As for the four−terminal tandem device, the top PVSK solar cell is measured using the same setup while the device is illuminated from the top DMD electrode; the bottom CIGS solar cell is measured with top PVSK device as the filter.

Conflict of Interest: The authors declare no competing financial interest.

Acknowledgment. This work was financially supported by the National Science Foundation (NSF-ECCS 1202231, Program Manager: Dr. Paul Werbos), Air Force Office of Scientific Research (Grant No. FA9550-12-1-0074, Program Manager: Dr. C. Lee). We also thank the technical support and discussions from Mr. Chun-Chiang Kuo, Dr. Jingbi You, Dr. Ziruo Hong, Dr. Gang Li, and Mr. Lei Meng.

Supporting Information Available: SEM image of the PVSK film on top of TiO_2; IV curves of the regular PVSK solar cell; Device stacking schematic for the four-terminal tandem device. The Supporting Information is available free of charge on the ACS Publications website at DOI: 10.1021/acsnano.5b03189.

REFERENCES AND NOTES

1. Li, G.; Zhu, R.; Yang, Y. Polymer Solar Cells. *Nat. Photonics* **2012**, *6*, 153–161.
2. Li, Y. Molecular Design of Photovoltaic Materials for Polymer Solar Cells: Toward Suitable Electronic Energy Levels and Broad Absorption. *Acc. Chem. Res.* **2012**, *45*, 723–733.
3. Liang, Y.; Yu, L. A New Class of Semiconducting Polymers for Bulk Heterojunction Solar Cells with Exceptionally High Performance. *Acc. Chem. Res.* **2010**, *43*, 1227–1236.
4. Li, G.; Shrotriya, V.; Huang, J.; Yao, Y.; Moriarty, T.; Emery, K.; Yang, Y. High-Efficiency Solution Processable Polymer Photovoltaic Cells by Self-Organization of Polymer Blends. *Nat. Mater.* **2005**, *4*, 864–868.
5. Yang, Y.; Chen, W.; Dou, L.; Chang, W.-H.; Duan, H.-S.; Bob, B.; Li, G.; Yang, Y. High-Performance Multiple-Donor Bulk Heterojunction Solar Cells. *Nat. Photonics* **2015**, *9*, 190–198.
6. You, J.; Dou, L.; Yoshimura, K.; Kato, T.; Ohya, K.; Moriarty, T.; Emery, K.; Chen, C.-C.; Gao, J.; Li, G.; Yang, Y. A Polymer Tandem Solar Cell with 10.6% Power Conversion Efficiency. *Nat. Commun.* **2013**, *4*, 1446.
7. Chung, I.; Lee, B.; He, J.; Chang, R. P. H.; Kanatzidis, M. G. All-Solid-State Dye-Sensitized Solar Cells with High Efficiency. *Nature* **2012**, *485*, 486–489.
8. Daeneke, T.; Kwon, T.-H.; Holmes, A. B.; Duffy, N. W.; Bach, U.; Spiccia, L. High-Efficiency Dye-Sensitized Solar Cells with Ferrocene-Based Electrolytes. *Nat. Chem.* **2011**, *3*, 211–215.
9. Grätzel, M. Recent Advances in Sensitized Mesoscopic Solar Cells. *Acc. Chem. Res.* **2009**, *42*, 1788–1798.
10. Wang, M.; Chamberland, N.; Breau, L.; Moser, J.-E.; Humphry-Baker, R.; Marsan, B.; Zakeeruddin, S. M.; Grätzel, M. An Organic Redox Electrolyte to Rival Triiodide/Iodide in Dye-Sensitized Solar Cells. *Nat. Chem.* **2010**, *2*, 385–389.
11. Green, M. A.; Ho-Baillie, A.; Snaith, H. J. The Emergence of Perovskite Solar Cells. *Nat. Photonics* **2014**, *8*, 506–514.
12. Heo, J. H.; Im, S. H.; Noh, J. H.; Mandal, T. N.; Lim, C.-S.; Chang, J. A.; Lee, Y. H.; Kim, H.-j.; Sarkar, A.; NazeeruddinMd, K.; et al. Efficient Inorganic-Organic Hybrid Heterojunction Solar Cells Containing Perovskite Compound and Polymeric Hole Conductors. *Nat. Photonics* **2013**, *7*, 486–491.
13. Lin, Q.; Armin, A.; Nagiri, R. C. R.; Burn, P. L.; Meredith, P. Electro-Optics of Perovskite Solar Cells. *Nat. Photonics* **2015**, *9*, 106–112.
14. Liu, D.; Kelly, T. L. Perovskite Solar Cells with a Planar Heterojunction Structure Prepared Using Room-Temperature Solution Processing Techniques. *Nat. Photonics* **2014**, *8*, 133–138.
15. Liu, M.; Johnston, M. B.; Snaith, H. J. Efficient Planar Heterojunction Perovskite Solar Cells by Vapour Deposition. *Nature* **2013**, *501*, 395–398.
16. Park, N.-G. Organometal Perovskite Light Absorbers Toward a 20% Efficiency Low-Cost Solid-State Mesoscopic Solar Cell. *J. Phys. Chem. Lett.* **2013**, *4*, 2423–2429.
17. Zhou, H.; Chen, Q.; Li, G.; Luo, S.; Song, T.-b.; Duan, H.-S.; Hong, Z.; You, J.; Liu, Y.; Yang, Y. Interface Engineering of Highly Efficient Perovskite Solar Cells. *Science* **2014**, *345*, 542–546.
18. Chen, Q.; Zhou, H.; Hong, Z.; Luo, S.; Duan, H.-S.; Wang, H.-H.; Liu, Y.; Li, G.; Yang, Y. Planar Heterojunction Perovskite Solar Cells *via* Vapor-Assisted Solution Process. *J. Am. Chem. Soc.* **2014**, *136*, 622–625.
19. You, J.; Hong, Z.; Yang, Y.; Chen, Q.; Cai, M.; Song, T.-B.; Chen, C.-C.; Lu, S.; Liu, Y.; Zhou, H.; et al. Low-Temperature Solution-Processed Perovskite Solar Cells with High Efficiency and Flexibility. *ACS Nano* **2014**, *8*, 1674–1680.
20. You, J.; Yang, Y.; Hong, Z.; Song, T.-B.; Meng, L.; Liu, Y.; Jiang, C.; Zhou, H.; Chang, W.-H.; Li, G.; et al. Moisture Assisted Perovskite Film Growth for High Performance Solar Cells. *Appl. Phys. Lett.* **2014**, *105*, 183902.
21. Xiao, Z.; Dong, Q.; Bi, C.; Shao, Y.; Yuan, Y.; Huang, J. Solvent Annealing of Perovskite-Induced Crystal Growth for Photovoltaic-Device Efficiency Enhancement. *Adv. Mater.* **2014**, *26*, 6503–6509.
22. Mitzi, D. B. Synthesis, Structure, and Properties of Organic-Inorganic Perovskites and Related Materials. *Prog. Inorg. Chem.* **2007**, 1–121.
23. Dou, L.; Yang, Y.; You, J.; Hong, Z.; Chang, W.-H.; Li, G.; Yang, Y. Solution-Processed Hybrid Perovskite Photodetectors with High Detectivity. *Nat. Commun.* **2014**, *5*, No. 5404.

24. Song, T.-B.; Chen, Q.; Zhou, H.; Luo, S.; Yang, Y.; You, J.; Yang, Y. Unraveling Film Transformations and Device Performance of Planar Perovskite Solar Cells. *Nano Energy* **2015**, *12*, 494–500.
25. Song, T.-B.; Chen, Q.; Zhou, H.; Jiang, C.; Wang, H.-H.; Yang, Y.; Liu, Y.; You, J.; Yang, Y. Perovskite Solar Cells: Film Formation and Properties. *J. Mater. Chem. A* **2015**, *3*, 9032–9050.
26. Xing, G.; Mathews, N.; Lim, S. S.; Yantara, N.; Liu, X.; Sabba, D.; Grätzel, M.; Mhaisalkar, S.; Sum, T. C. Low-Temperature Solution-Processed Wavelength-Tunable Perovskites for Lasing. *Nat. Mater.* **2014**, *13*, 476–480.
27. De Wolf, S.; Holovsky, J.; Moon, S.-J.; Löper, P.; Niesen, B.; Ledinsky, M.; Haug, F.-J.; Yum, J.-H.; Ballif, C. Organometallic Halide Perovskites: Sharp Optical Absorption Edge and Its Relation to Photovoltaic Performance. *J. Phys. Chem. Lett.* **2014**, *5*, 1035–1039.
28. Umari, P.; Mosconi, E.; De Angelis, F. Relativistic GW Calculations on $CH_3NH_3PbI_3$ and $CH_3NH_3SnI_3$ Perovskites for Solar Cell Applications. *Sci. Rep.* **2014**, *4*, No. 4467.
29. Gao, P.; Gratzel, M.; Nazeeruddin, M. K. Organohalide Lead Perovskites for Photovoltaic Applications. *Energy Environ. Sci.* **2014**, *7*, 2448–2463.
30. Eperon, G. E.; Burlakov, V. M.; Goriely, A.; Snaith, H. J. Neutral Color Semitransparent Microstructured Perovskite Solar Cells. *ACS Nano* **2014**, *8*, 591–598.
31. Wu, H.; Kong, D.; Ruan, Z.; Hsu, P.-C.; Wang, S.; Yu, Z.; Carney, T. J.; Hu, L.; Fan, S.; Cui, Y. A Transparent Electrode Based on a Metal Nanotrough Network. *Nat. Nanotechnol.* **2013**, *8*, 421–425.
32. Mao, L.; Chen, Q.; Li, Y.; Li, Y.; Cai, J.; Su, W.; Bai, S.; Jin, Y.; Ma, C.-Q.; Cui, Z.; et al. Flexible Silver Grid/PEDOT:PSS Hybrid Electrodes for Large Area Inverted Polymer Solar Cells. *Nano Energy* **2014**, *10*, 259–267.
33. Li, Y.; Mao, L.; Gao, Y.; Zhang, P.; Li, C.; Ma, C.; Tu, Y.; Cui, Z.; Chen, L. ITO-Free Photovoltaic Cell Utilizing a High-Sesolution Silver Grid Current Collecting Layer. *Sol. Energy Mater. Sol. Cells* **2013**, *113*, 85–89.
34. Song, T.-B.; Chen, Y.; Chung, C.-H.; Yang, Y.; Bob, B.; Duan, H.-S.; Li, G.; Tu, K.-N.; Huang, Y.; Yang, Y. Nanoscale Joule Heating and Electromigration Enhanced Ripening of Silver Nanowire Contacts. *ACS Nano* **2014**, *8*, 2804–2811.
35. Roldan-Carmona, C.; Malinkiewicz, O.; Betancur, R.; Longo, G.; Momblona, C.; Jaramillo, F.; Camacho, L.; Bolink, H. J. High Efficiency Single-Junction Semitransparent Perovskite Solar Cells. *Energy Environ. Sci.* **2014**, *7*, 2968–2973.
36. Bryant, D.; Greenwood, P.; Troughton, J.; Wijdekop, M.; Carnie, M.; Davies, M.; Wojciechowski, K.; Snaith, H. J.; Watson, T.; Worsley, D. A Transparent Conductive Adhesive Laminate Electrode for High-Efficiency Organic-Inorganic Lead Halide Perovskite Solar Cells. *Adv. Mater.* **2014**, *26*, 7499–7504.
37. Battaglia, C.; Yin, X.; Zheng, M.; Sharp, I. D.; Chen, T.; McDonnell, S.; Azcatl, A.; Carraro, C.; Ma, B.; Maboudian, R.; et al. Hole Selective MoO_x Contact for Silicon Solar Cells. *Nano Lett.* **2014**, *14*, 967–971.
38. Zilberberg, K.; Gharbi, H.; Behrendt, A.; Trost, S.; Riedl, T. Low-Temperature, Solution-Processed MoO_x for Efficient and Stable Organic Solar Cells. *ACS Appl. Mater. Interfaces* **2012**, *4*, 1164–1168.
39. Jin, H.; Tao, C.; Velusamy, M.; Aljada, M.; Zhang, Y.; Hambsch, M.; Burn, P. L.; Meredith, P. Efficient, Large Area ITO-and-PEDOT-Free Organic Solar Cell Sub-Modules. *Adv. Mater.* **2012**, *24*, 2572–2577.
40. Yambem, S. D.; Ullah, M.; Tandy, K.; Burn, P. L.; Namdas, E. B. ITO-Free Top Emitting Organic Light Emitting Diodes with Enhanced Light Out-Coupling. *Laser Photonics Rev.* **2014**, *8*, 165–171.
41. Della Gaspera, E.; Peng, Y.; Hou, Q.; Spiccia, L.; Bach, U.; Jasieniak, J. J.; Cheng, Y.-B. Ultra-Thin High Efficiency Semitransparent Perovskite Solar Cells. *Nano Energy* **2015**, *13*, 249–257.
42. Janković, V.; Yang, Y.; You, J.; Dou, L.; Liu, Y.; Cheung, P.; Chang, J. P.; Yang, Y. Active Layer-Incorporated, Spectrally Tuned Au/SiO_2 Core/Shell Nanorod-Based Light Trapping for Organic Photovoltaics. *ACS Nano* **2013**, *7*, 3815–3822.
43. Hou, W. W.; Bob, B.; Li, S.-h.; Yang, Y. Low-Temperature Processing of a Solution-Deposited CuInSSe Thin-Film Solar Cell. *Thin Solid Films* **2009**, *517*, 6853–6856.
44. Bailie, C. D.; Christoforo, M. G.; Mailoa, J. P.; Bowring, A. R.; Unger, E. L.; Nguyen, W. H.; Burschka, J.; Pellet, N.; Lee, J. Z.; Gratzel, M.; et al. Semi-Transparent Perovskite Solar Cells for Tandems with Silicon and CIGS. *Energy Environ. Sci.* **2015**, *8*, 956–963.